Estimation of biogenic volatile organic compound (BVOC) emissions from the terrestrial ecosystem in China using real-time remote sensing data

M. Li, X. Huang, J. Li and Y. Song*

State Key Joint Laboratory of Environmental Simulation and Pollution Control, Department of Environmental Science, Peking University, Beijing 100871, China

* Corresponding author: songyu@pku.edu.cn

Abstract

Because of the high emission rate and reactivity, biogenic volatile organic compounds (BVOCs) play a significant role in the terrestrial ecosystems, human health, secondary pollution, global climate change and the global carbon cycle. Past estimations of BVOC emissions in China on the national scale were based on outdated empirical algorithms suggested around 10 years ago and coarsely-resolved meteorological data, and there have been significant aging of the land surface parameters in dynamic meteorological models and BVOC estimation models, leading to large inaccuracies in the estimated results. To refine BVOC emission estimations for China, we used the latest algorithms of MEGAN (Model of Emissions of Gases and Aerosols from Nature), with modified MM5 (the Fifth-Generation Mesoscale Model) providing highly resolved meteorological data, to estimate the biogenic emissions of VOCs for China in 2006. Real-time MODIS (Moderate Resolution Imaging Spectroradiometer) land-use and vegetative cover data were introduced in MM5 to

replace the land surface parameters and to improve the simulation performance of MM5. Highly-resolved 8-day MODIS leaf area index (LAI) data were also used to determine the influence of LAI and leaf age deviation from standard conditions. In this study, the annual BVOC emissions for the whole country totaled 13.02 Tg C, higher than the recent estimation of Tie et al. (2006) by 19.9%, which might be attributed to the aged land-surface data and meteorological input, as indicated by several case studies, and higher than Klinger et al. (2002) by 72.9%. Therein, the most important individual contributor was isoprene (9.39 Tg C yr^{-1}), followed by α-pinene (1.24 Tg C yr^{-1}) and β-pinene (0.81 Tg C yr^{-1}). Spatially, isoprene emission was concentrated in South China, which is covered by large areas of broadleaf forests and shrubs. While Southeast China was the top-ranking contributor of monoterpenes, in which the dominant vegetation genera consist of coniferous forests. In the main southern cities (Fujian, Guangxi, Hainan, Hunan, Jiangxi, and Yunnan), Shaanxi and Inner Mongolia, BVOC emissions predominated over anthropogenic NMVOC emissions. Temporally, BVOC emissions primarily occurred in July and August, with daily emissions peaking at about 13:00~14:00 hours (Beijing Time, BJT).

1 Introduction

Large quantities of non-methane volatile organic compounds (NMVOCs) are emitted from various anthropogenic and natural sources, such as vegetation, marine algae (McKay et al., 1996) and microbiological decomposition (Kuzma et al., 1995; Zemankova and Brechler, 2010). On the global scale, natural emissions of NMVOCs exceed anthropogenic emissions, nearly by an order of magnitude (Benkovitz et al., 2004). On the regional scale, although anthropogenic sources usually dominate in urban areas, in many cases, BVOCs made significant contributions to the overall VOC inventories of both urban and rural areas (Benjamin et al., 1997).

The importance of BVOCs in tropospheric physics and chemistry was first acknowledged about 50 years ago (Went, 1960) . First, many BVOC species are emitted in copious quantities and strongly influence the composition of the troposphere (Guenther et al., 1999; Monks et al., 2009). In particular, isoprene and monoterpenes are thought to be the dominant BVOC species (Kesselmeier and Staudt, 1999; Goldstein and Galbally, 2009; Monks et al., 2009). Second, many BVOC species are of extremely high reactivity with tropospheric oxidants. Through their oxidation, BVOCs can significantly change the oxidizing capacity of the atmosphere, and thus affecting local and global air quality (Ryerson et al., 2001; Wiedinmyer et al., 2004; Arneth et al., 2008; Goldstein and Galbally, 2009; Hallquist et al., 2009; Monks et al., 2009). Third, BVOCs, through complex oxidation processes, have also been implicated as key precursors to biogenic secondary organic aerosol (BSOA), thereby providing an additional burden of aerosol in the atmosphere and further exerting a strong influence

on global climate-related issues (Griffin et al., 1999; Atkinson and Arey, 2003; Kanakidou et al., 2005; Szidat et al., 2006; Goldstein and Galbally, 2009; Hallquist et al., 2009; Pacifico et al., 2009; Perraud et al., 2011). Finally, many studies have also concluded that reactive BVOCs were important source of carbon budget and have significant implications for the global carbon (C) cycle (Kesselmeier et al., 2002; Streets et al., 2003; Karl et al., 2009).

To further explore the roles of BVOCs, it is essential to accurately estimate time- and space-resolved BVOC emissions. The most important emitter of BVOCs is vegetation, especially forest ecosystems (Zemankova and Brechler, 2010). China is a country that encompasses large areas covered by a variety of plants. In recent decades, studies have been conducted in China focused on the development of national or regional BVOC emission inventories based on various models or approaches, which reported a wide emission range of 4.06~16.43 Tg C yr^{-1} for isoprene and 1.84~4.46 Tg C yr^{-1} for monoterpenes on the national level (Guenther et al., 1995; Klinger et al., 2002; Olivier et al., 2003; Wang et al., 2003; Granier et al., 2005; Guenther et al., 2006; Tie et al., 2006; Arneth et al., 2007; Wang et al., 2007; Schurgers et al., 2009; Leung et al., 2010; Zheng et al., 2010; Wang et al., 2011).

However, past estimations were deficient with regard to estimation algorithms and input data. (1) In terms of methodology, the past studies did not fully quantify the factors controlling BVOC emissions, such as LAI and leaf age. Some studies assumed the emissions of monoterpenes and other reactive VOCs to be solely temperature dependent, failing to recognize their dependence on light (Wang et al., 2003; Zheng et

al., 2010). (2) In addition, some estimates used outdated USGS (United States Geological Survey) land-cover data to identify vegetation distributions and/or to drive the dynamic meteorological model (Tie et al., 2006; Wang et al., 2011), which might result in the misidentification of plant function types (PFTs) and large uncertainties in the simulated meteorological results, as indicated by many studies (Molders, 2001; Atkinson, 2003). Many studies have also highlighted the potential of satellite data to replace the land-surface parameters and improve simulation performance in dynamical meteorological models (Gutman and Ignatov, 1998; Crawford et al., 2001; Kurkowski et al., 2003; de Foy et al., 2006; Yucel, 2006; Ge et al., 2008; Meng et al., 2009). (3) Thirdly, many studies were based on coarsely-resolved meteorological data interpolated from daily or monthly weather datasets, leading to coarse resolutions of emission inventories (for example $0.5° \times 0.5°$ in studies by Guenther et al. (2006)) and failures to capture the extreme emission values (Ashworth et al., 2010). Additionally, the use of an early version of monthly MODIS LAI product (Guenther et al., 2006) was another source of uncertainty. Consequently, all the factors above jointly led to large uncertainties and great variations among the results of past studies.

In this work, we aimed to estimate the amounts, spatial distributions and temporal variations of BVOC emissions from the terrestrial ecosystems of China in 2006 using MODIS-MM5-MEGAN, with modified MM5 providing hourly meteorological outputs to drive the estimations. Real-time MODIS data were introduced into MM5 to modify the land surface parameters and improve the simulation performance, and were also used to provide a highly resolved input database for the calibration and estimation of

BVOC emissions. Two primary classes of BVOCs, isoprene (C_5H_8) and monoterpenes ($C_{10}H_{16}$), including a group of α-pinene, β-pinene, limonene, myrcene, sabinene, 3-carene and ocimene, were considered in this study.

2 Methods and Data

2.1 BVOC emission algorithms and data

We estimated BVOC emissions based on the parameterized canopy environment emission activity (PCEEA) algorithms in MEGAN, described by Guenther et al. (2006) and Sakulyanontvittaya et al. (2008), as shown schematically in Fig. 1.

The net BVOC emission fluxes (mg m^{-2} h^{-1}) into the above-canopy atmosphere were empirically specified according to Eq. (1)

$$Emission = EF \times \gamma_T \times [(1 - LDF) + LDF \times \gamma_P] \times \gamma_{LAI} \times \gamma_{age} \times \gamma_{SM} \times \rho \quad (1)$$

where EF (mg m^{-2} h^{-1}) is a standard canopy-scale emission factor, which represents the BVOC emission rates under standard conditions. Global gridded EFs for isoprene and seven monoterpene species, with a base resolution of 30 s for the year 2000, were downloaded from the CDP (Community Data Portal) website (http://cdp.ucar.edu/).

Changes in BVOC emissions due to deviations from standard conditions were modified through a set of dimensionless emission activity factors (γ_T, γ_P, γ_{age}, γ_{LAI}, γ_{SM} and ρ). The light dependence of the BVOC emission processes was considered using the light-dependent function (LDF). In our estimations, the influences of soil moisture and detailed canopy information were neglected; thus, γ_{SM} and ρ, which represent the influence of soil moisture and production and loss of BVOCs within the canopy,

126 respectively, were set to 1. Detailed information and calculation processes for all
127 correction terms can be found in the published reports of Guenther et al. (2006) and
128 Sakulyanontvittaya et al. (2008), so no further details are provided here.

129 Highly resolved meteorological outputs of air temperatures at 2 m (T2) and solar
130 shortwave radiation (SWDOWN) (Fig. 2) from MM5 were used to estimate the light
131 and temperature dependencies (γ_T and γ_P) of BVOC emissions. The horizontal
132 resolution of the modeling domain was 12 km × 12 km, centered at (37.40 °N,
133 102.52 °E) with 440 × 380 cells in the horizontal direction and 35 layers in the vertical
134 direction. The Four Dimensional Data Assimilation (FDDA) scheme coupled with
135 NCEP/FNL data was included in our simulation to refine model performance. MM5
136 was run for the entire year of 2006, and each run covered 3.5 days with 12-hour spin-up
137 time.

138 In MEGAN, by default the modifications of LAI and leaf age were based on an
139 early version of monthly MODIS LAI product for the year 2003, which were
140 coarsely-resolved and deficient in the retrieval algorithms (Garrigues et al., 2008).
141 Additionally, the LAI distributions might show considerable inter-annual variations
142 and influence BVOC emissions (Warneke et al., 2010). Therefore, in this study the
143 substantially improved MODIS LAI data (MCD15A2) (Fig. 2) based on revised
144 satellite measurements for the specific year 2006 (Garrigues et al., 2008; Warneke et al.,
145 2010), with a spatial resolution of 1 km and a higher temporal resolution of
146 8-day(Justice et al., 2002), were introduced in MEGAN to estimate the influences of
147 LAI (γ_{LAI}) and leaf age (γ_{age}) on BVOC emission capacities.

2.2 Modifications of land surface parameters in MM5

Accurate simulations of meteorological fields are important for the estimation of BVOC emissions. It is now widely recognized that several key land surface parameters, including land cover, vegetation fraction (VGF) et al. significantly affect land-atmosphere interactions and are thus important in weather simulations (Wittich and Hansing, 1995; Crawford et al., 2001; de Foy et al., 2006; Yucel, 2006).

By default, MM5 uses the USGS global 1 km land-use data derived from the AVHRR (Advanced Very High Resolution Radiometer) observation, which is based on 1-year data from April 1992 to March 1993. And the VGF data in MM5 are derived from monthly AVHRR NDVI (Normalized Difference Vegetation Index) data at a resolution of 10 min (de Foy et al., 2006; Meng et al., 2009).

However, over the last decade, global terrestrial ecosystems underwent great changes, such as urbanization, desertification and deforestation, causing the existing land-surface data in MM5 to be outdated and, thus, likely to produce errors in weather simulations (Pielke et al., 2002; Yucel, 2006). By far, many studies have been conducted to replace land surface data in meteorological models with satellite data (Crawford et al., 2001; Kurkowski et al., 2003; Tian et al., 2004; de Foy et al., 2006). Studies also reasoned that the global coverage, enhanced resolutions and accurate calibrations for retrievals of MODIS land surface data have great advantages over AVHRR (Justice et al., 2002). In this study, we introduced the latest MODIS land products to replace the land-surface parameters (land-use and VGF) in MM5.

MODIS land-use data (MCD12Q1) for the year 2006 and water mask data

(MOD44W) for the year 2000, both with a resolution of 500 m (Justice et al., 2002), were used to obtain a new land-use map by mapping the 17 MODIS land-use categories defined by the International Geosphere-Biosphere Program (IGBP) onto the existing 24 USGS categories, as shown in Table 1. The coverage fraction of each land use type in each grid cell was also calculated based on the new land use map. To validate the accuracy of the MODIS land-use data, the 1:100, 0000 plant distribution map (Fig. 3c), which is based on local field surveys from the Plant Research Institute of the Chinese Academy of Sciences, was used for comparison. According to the USGS data, South China was covered by large areas of crops (Fig. 3a), while MODIS observations found that South China contained mixed forest, grass and shrubs, showing a similar distribution patterns with plant distributions obtained from field investigations (Fig. 3b). Therefore, we concluded that the MODIS land-use data better reflects the present land cover characteristics of China and may help to improve the simulations.

In this study, the VGF in MM5 was calculated from MODIS NDVI data (MOD13A2), giving monthly NDVI at 1 km resolution (Justice et al., 2002). Previous studies indicated linear (Wittich and Hansing, 1995; Gutman and Ignatov, 1998; de Foy et al., 2006) or nonlinear relationships (Purevdorj et al., 1998; Jakubauskas et al., 2000; Jiang et al., 2010) between NDVI and VGF. Here, we derived the value of VGF based on Eq. (2) and (3), as recommended by Dr. de Foy (private correspondence).

$$VGF = 1.5 \times (NDVI - 0.1) \quad (NDVI < 0.547) \tag{2}$$

$$VGF = 3.2 \times NDVI - 1.08 \quad (NDVI \geq 0.547) \tag{3}$$

3 Results and Discussions

3.1 Evaluation of MM5 output

The observed surface temperature of 378 sites in China provided by the National Climatic Data Center (NCDC) (http://www.ncdc.noaa.gov/), available with a temporal resolution of an hour or three hours, and observed daily total radiation data of 89 sites in China downloaded from the China Meteorological Data Sharing Service System (http://cdc.cma.gov.cn/) were used to evaluate the simulation performance of T2 and SWDOWN. Simulated results are compared with observations in terms of performance statistics, spatial distribution and temporal variations.

3.1.1 Statistical analysis

To investigate the model's performance during different simulation periods, the statistical analyses of T2 and SWDOWN for four seasons were displayed in Table 2, respectively. Overall, the meteorological conditions simulated by MM5 were desirable for driving MEGAN.

Overestimations of T2 occurred in summer, with a warm bias of 0.67 ℃ and underestimations occurred in the other three seasons, with a cold bias of 0.56 ℃, 0.56 ℃ and 0.62 ℃ respectively for spring, autumn and winter, which resulted in NMB of -2% and MB of -0.26℃ for the whole year.

In general, simulated downward shortwave radiation is larger than the observed data all the year, probably due to that MM5 didn't account for the absorbing and scattering solar radiation (Chen and Dudhia, 2001). The mean bias for SWDOWN was respectively 26.63, 27.40, 12.03 and 9.81 W m^{-2} for spring, summer, autumn and winter,

214 which resulted in an average yearly bias (MB) of 18.28 W m^{-2}.

215 **3.1.2 Spatial-temporal distributions**

216 Fig. 2 shows the spatial distribution of simulated seasonally average T2 and
217 SWDOWN. In general, the simulation of MM5 reproduced the spatial characteristics of
218 T2 and SWDOWN (the distribution of observed values are not shown here). The spatial
219 distribution patterns of temperature were typical for all the four seasons and generally
220 decreased from the south to the north and from the east to the west, consistent with
221 terrain heights and latitudes. The spatial distribution of solar radiation roughly
222 decreased from the northwest to the southeast, influenced by latitude, terrain height and
223 climate change. On average, the solar radiation reached a high value center near the
224 Tibetan Plateau, while the low value center occurred near the Sichuan Basin (Fig. 2),
225 influenced by the enclosed terrain and the abundant water vapor in the atmosphere.

226 The seasonal variation of observed T2 and solar radiation is overall captured. On
227 the whole, 2 m air temperature was highest in summer, followed by spring and autumn,
228 and then winter, while the solar radiation energy was highest in summer, followed by
229 spring and then autumn and winter (Fig. 2).

230 **3.2 BVOC emission budgets**

231 Hourly emissions of isoprene and seven monoterpene species in China were
232 calculated for the year 2006, with a spatial resolution of 12 km × 12 km. In the
233 following section, all the results were measured as carbon weights of the constituent
234 compounds, unless stated otherwise.

235 Because of the distinct reactivities of BVOC species, a better understanding of the

236 relative contributions for individual BVOC species may be critical for further
237 exploration of secondary products of BVOCs and the determination of appropriate
238 regulatory oxidant control strategies (Hoffmann et al., 1997; Wiedinmyer et al., 2004;
239 Hallquist et al., 2009).

240 Seasonal and annual total emission budgets determined by this study are listed in
241 Table 3. As shown, the annual BVOC emissions totaled 13.02 Tg C (which equals
242 14.76 Tg compound). Regarding the relative contributions of individual species, the
243 dominant contributor was isoprene, with an annual emission budget of 9.39 Tg C,
244 accounting for approximately 72% of the total BVOC budget. The next most
245 predominant contributor was α-pinene (1.24 Tg C yr^{-1}), which was responsible for 9.5%
246 of the total BVOC emissions and 34.1% of the total monoterpene emissions, followed
247 by β-pinene (0.81 Tg C yr^{-1}) and 3-carene (0.68 Tg C yr^{-1}). The other four monoterpene
248 species were less significant, and the annual emission budgets on the national scale
249 were as follows: ocimene (0.32 Tg C), limonene (0.28 Tg C), sabinene (0.19 Tg C) and
250 myrcene (0.11 Tg C). Overall, the annual emission budget of monoterpenes was 3.63
251 Tg C, which was approximately one-third that of isoprene.

252 Compared to the global emission estimations by Guenther et al. (2006), the annual
253 emissions of isoprene in China was responsible for 2.0 % of global emissions (462.7 Tg
254 C), while monoterpenes accounted for 4.3 % of global emissions (85.3 Tg C). Although
255 China covered approximately 6% of the global land area, it only contributed 2.4% to
256 global BVOC emissions. Currently, China is undergoing rapid land-cover change and is
257 now the world's leading nation in existing plantation area (24% of the global total)

(Geron et al., 2006) and implying a greater future impact on BVOC emission contributions.

3.3 Spatial distributions of BVOC emission fluxes

As described in section 2.1, the spatial distribution of BVOC emission fluxes (expressed as the total emission of BVOCs per unit area, per unit time) depended on the distribution of tree species and meteorological conditions.

As shown in Fig. 3, forests and shrubs were mainly distributed in Northeast and South China. According to the survey results from the Plant Research Institute, Northeast China was primarily covered by deciduous coniferous forests (mainly *Larix gmelini*) and deciduous broadleaf forests (mainly *Quercus mongolica, Tilia Mongolia* and *Betula platyphylla*). By comparison, the distribution pattern of tree species in South China was more complex. Large areas of evergreen coniferous forests (mainly *Pinus massoniana* and *Cunninghamia lanceolata*) and shrubs were found in Southeast China, while the main plant genera in Southwest China were larger groups of evergreen tree species, including evergreen broadleaf forests (e.g. *Quercus aquifolioides*), evergreen coniferous forests (*Picea likiangensis var.b*alfouriana and *Pinus yunnanensis*) and shrubs. Notably, large areas of tropical rain forests were concentrated in the southeast of Tibet and south of Yunnan Province. Additionally, high fractional cover of deciduous broadleaf forests (mainly *Quercus variabilis* and *Quercus liaotungensis*) was found south of Shaanxi.

The field measurements of previous studies indicated that broadleaf forests (especially *Quercus*, *Populus* and *Eucalyptus*) and shrubs were of high isoprene

emission capacities, while the intense emission of monoterpenes generally corresponded to the dense distribution of coniferous forests (especially *Pinus* and *Picea*). Crops and grass were considered to have low BVOC emitting capacities (Kesselmeier and Staudt, 1999; Wang et al., 2003; Guenther et al., 2006; Wang et al., 2007; Sakulyanontvittaya et al., 2008; Karl et al., 2009; Zheng et al., 2010; Wang et al., 2011). Correspondingly, the spatial distributions of standard emission factors presented in Fig. 4 (in which blank areas represent districts with no plant cover), were consistent with the plant distributions in China (Fig. 3). Specifically, plants in the northeast and south of China as well as in the south of Shaanxi exhibited high isoprene emission capacities (Fig. 4a). High monoterpene emission capacities were found in the northeast and southeast of China as well as the Sichuan-Tibet area (Fig. 4b).

As illustrated in Fig. 5, the distribution patterns of biogenic emissions modified by real conditions agreed well with those under standard conditions (Fig. 4). The high EFs as well as the low latitude and resulting high temperature in the south of China led to strong isoprene emission there (Fig. 5a). High isoprene emission flux values were also found in the south of Shaanxi. Although the isoprene emission capacities of plants in Northeast China were extremely high (Fig. 5a), the real average emission flux values were relatively low (Fig. 5a), partly due to the relative low temperature throughout the year. Additionally, as mentioned above, Northeast China was mainly covered by deciduous forests that cease to grow and nearly emit no isoprene in winter. High monoterpene emission flux values were centered in the south (especially the southeast) of China, where a high density of coniferous forests were concentrated (Fig. 3c). In

Southwest China, especially the Sichuan-Tibet area, the high altitude and resulting low temperature (Fig. 2) of the Tibetan Plateau led to relatively low emission flux.

The lowest BVOC emissions occurred in Northwest China (Fig. 5), which is primarily covered by barren land and low emitting grass (Fig. 3). In North China and the north of East China region, which is mainly covered by crops (Fig. 3), BVOC emissions were also negligible (Fig. 5).

3.4 Province-specific emission

Province-level emission contribution depended on plant distribution, forested area, climatic conditions, and so forth. Detailed information depicting plant cover by province, listed in Table S1, was based on tree species data from the Chinese Academy of Sciences.

The top-ranking isoprene contributor was Yunnan, with approximately 0.90 Tg C emitted yearly, followed by Hunan (0.75 Tg C yr^{-1}), and Sichuan and Guangxi (both 0.66 Tg C yr^{-1}). The four provinces, which respectively contributed 9.6%, 8.0%, 7.0% and 7.0% to the total isoprene emissions, all have dense plant cover. Take Yunnan Province for instance. Yunnan had approximately 11.0×10^4 km^2 of forests, accounting for 28.7% of its land area (Table S1). Subtropical evergreen broadleaf forests were also common in Yunnan, accounting for approximately 28.2% (3.1×10^4 km^2) of the forested area. Moreover, Yunnan was also covered by large areas of shrubs (8.6×10^4 km^2) (Table S1). The high isoprene emission capacities of broadleaf forests and shrubs led to the strong emission of isoprene in Yunnan. However, our results also depicted a contradiction between the extremely high forest and shrub coverage (30.1×10^3 km^2 of

broadleaf forests and 108.4 × 10^3 km^2 of shrubs) and the relatively low isoprene contribution in Sichuan Province. As mentioned above, this phenomenon could result from the low temperatures (Fig. 2) (due to terrain height) in the west of Sichuan and the low solar radiation (Fig. 2) in the east of Sichuan, combined with the enclosed terrain and the abundant cloudiness in the atmosphere.

The emission rates of monoterpenes were in general agreement with the distribution of coniferous forests. Specifically, Guangxi and Yunnan Province were the highest emitters, with an annual emission budget of 0.36 Tg C (totally contributing 19.8% to the annual emission of monoterpenes), followed by Hunan (0.30 Tg $C.yr^{-1}$, 8.2%) (Table 4).

In determining regional environmental strategies, province-specific BVOC emissions can provide constructive information for local administrations to make effective environmental decisions associated with oxidant control strategies and urban greening programs (Schell et al., 2001; Liao et al., 2007; Leung et al., 2010).

3.5 Temporal variations in BVOC emissions

There is increasing evidence that the seasonal changes of meteorological conditions and plant phenology greatly affect fluctuations in BVOC emission. Thus, seasonal variations must be considered to achieve an accurate estimation of vegetative BVOC emissions.

Isoprene emissions were highest throughout the country in the summer and there were fewer spatial differences in emission distributions (Fig. 6b). In winter, the LAI values decreased dramatically with the loss of leaves in deciduous forests, particularly

346 in Northeast China (Fig. 6d). By comparison, in the southeast and southwest of China,
347 the LAI values remained high throughout the year (Fig. 2) because of the prevalence of
348 tropical and subtropical evergreen forests. However, the low temperatures and low
349 solar radiation in winter (Fig. 2) still led to low BVOC emissions across China (Fig. 6d).
350 The spatial distribution patterns and seasonal variations of monoterpene emissions (Fig.
351 7) were similar to those of isoprene emissions, but the spatial variations were larger.

352 Fig. 8 shows the bell-shaped monthly evolution patterns of the total BVOC on a
353 national level as well as the monthly changes of LAI, temperature and solar radiation.
354 In general, BVOC emissions concentrated during April to October and peaked in July
355 with a monthly emission of 3.18 Tg C (Table 3). As the season transitioned with
356 accompanying decreases in temperature, radiation and vegetation, BVOC emission
357 intensities declined dramatically, reaching a lowest value of 0.10 Tg C in January
358 (Table 2). Monthly isoprene emissions fluctuated between a maximum (2.42 Tg C) in
359 July and a minimum (0.05 Tg C) in January. The same pattern was observed for
360 monoterpene emissions, for which a peak emission of 0.76 Tg C occurred in July and
361 the lowest emission (0.05 Tg C) occurred in winter.

362 In addition to seasonal changes, the temporal patterns of BVOC emissions
363 displayed obvious diurnal cycles. Biogenic isoprene emissions peaked at
364 approximately 13:00 (BJT) and nearly ceased during the night. In general, the diurnal
365 pattern of monoterpene emissions agreed with that of isoprene, with the strongest
366 emission occurring at about 14:00 (BJT). By comparison, the diurnal variation
367 observed for monoterpene emissions was much smaller than isoprene emissions and

maintained a relatively high level during the night. Many studies have pointed out that, isoprene oxidation is dominated by reactions with hydroxyl ($^{\cdot}OH$) during the day and reactions with nitrate radicals (NO_3) during the night (Atkinson and Arey, 2003; Monks et al., 2009). Thus, the strong diurnal cycles of BVOCs have direct effects on the formations and diurnal variations of ozone and SOA.

3.6 Comparisons to anthropogenic emissions

Recent studies proposed an interaction between BVOCs and AVOCs (anthropogenic volatile organic compounds) in the formation of SOA (Goldstein and Galbally, 2009). More important, because of the significant differences in the composition, reactivity and oxidation products, the regional variation of relative weights for BVOCs compared with AVOCs could affect local air quality and pollution controlling strategies (Lane and Pandis, 2007). Therefore, to further explore the role of BVOCs in atmospheric chemical processes, it is essential to compare BVOC emissions to anthropogenic emissions.

The inventory of AVOC emissions in 2006 was taken from the study by Zhang et al. (2009), which gave AVOC emissions for all the major anthropogenic sources (power, industry, residential and transportation) in China. In total, approximately 23.2 Tg NMVOCs (measured as full molecular weights of the constituent compounds) were emitted from China in 2006 (Zhang et al., 2009), leading to a total annual emission of NMVOCs for 37.96 Tg for the base year 2006. This value is approximately 1.6 times our estimate of natural emissions (14.76 Tg compound yr^{-1}). Guangdong made the largest contribution to NMVOC emissions, with an annual emission of 2.61 Tg,

followed by Sichuan (2.32 Tg yr^{-1}) and Shandong (2.21 Tg yr^{-1}). However, because of the complex plant distribution and economic structure across China, the relative ratio of BVOCs/AVOCs varied greatly by region.

The total amount of VOC emissions from natural and anthropogenic sources for each province is listed in Table 4. The distribution of anthropogenic NMVOC emissions was closely related to energy-consuming activities and population density, and reached a high value in the eastern area of China, while the distribution of BVOCs was closely dependent on plant distribution and centered in the south and northeast of China. Of the 32 provinces for which complete data were listed (the anthropogenic NMVOCs emission data of Taiwan was not available), BVOC emissions were comparable to anthropogenic emissions (the difference of the two sources was less than 0.02 Tg compound yr^{-1}) in Chongqing, Guizhou and Heilongjiang. Emissions of NMVOCs from natural or anthropogenic origins in western provinces, which were undeveloped and sparsely populated (e.g., Qinghai and Tibet), all maintained a negligible value. On the other hand, in the other eight provinces (including Fujian, Guangxi, Hainan, Hunan, Inner Mongolia, Jiangxi, Shaanxi, and Yunnan), where the plant cover fractions were high, BVOC emissions predominated over anthropogenic NMVOC emissions (Table 3), making it likely that BVOCs would play a more important role in local photochemistry processes and should not be ignored.

3.7 Comparisons with past studies

3.7.1 Comparisons of BVOC emission budgets

Because of the differences in algorithms and input data applied, our results may

differ greatly from previous published studies and it's important to compare the results for further improvement.

The results of this study fall in the range of past studies (Table 5). As shown in Table 5, the annual emission budgets estimated by the present study is higher than the results of Klinger et al. (2002) by 72.2% and lower than that of Guenther et al. (1995) by 32.8% (Table 5), which were all based on the outdated G95 algorithms (Guenther et al., 1995). In addition, Klinger et al. (2002) indicated a rather different province-level BVOC emission from ours (Fig. 9). Klinger et al. (2002) gave a higher emission value in the northern cities of China, for example, they estimated Inner Mongolia, mainly covered by *Quercus*, *Larix* and *Betula*, to be the dominant contributor to both isoprene and monoterpene emissions, while in our study its contribution was minor. Additionally, the results given by Klinger et al. (2002) can only reflect the natural emission level of vegetation during the last decade that might have changed dramatically by now due to land cover change.

Compared with the results of Tie et al. (2006), which are based on the algorithms of Guenther et al. (2000), our estimations of annual isoprene and monoterpene emissions were higher by 22% and 15%, respectively (Table 5). To further explore the main reasons resulting in the differences of the two studies, we conducted several case studies with the algorithms and EFs provided by Tie et al. (2006) as shown in Table 6. From comparisons between case 1 and case 2, it's clear that land-use played a dominant role in BVOC estimation. The use of MODIS land-use data (as in case 1) led to an increase of 45.5% and 34.1% for the emissions of isoprene and monoterpenes. Further,

434 we conduct a control trial by introducing the EFs of isoprene based on USGS land
435 cover in MEGAN (case 3) and the annual emissions dropped dramatically from 9.39 Tg
436 C to 4.27 Tg C nearly by a half. Hence, it's true that the use of USGS land-use
437 distribution in Tie et al. (2006) should be responsible for the underestimation of BVOC
438 emissions. The differences between the two works may also be explained, in part, by
439 the different meteorological simulation outputs given by WRF (Weather Research and
440 Forecasting) in Tie et al. (2006) and by MM5 in our study (case 2). However, the
441 increase of BVOC emissions in this study than Tie et al. (2006) were not so high as
442 expected, which can be attributed to the reduce of BVOC emissions by algorithms in
443 Guenther et al. (2006) (see case 2 and case 3).

444 The estimated isoprene emission in this study was comparable to that given for the
445 year 2000 by Guenther et al. (2006) based on similar algorithms, with a slight
446 underestimation of 6.2% (Table 5). But the estimated total emission of monoterpenes
447 was higher by 43.5% (Table 5) than Guenther et al. (2006), with a similar distribution
448 pattern.

449 In the past few years, many other highly-resolved global inventories have also
450 been developed within international projects based on various methods. The POET
451 (Precursors of Ozone and their Effects in the Troposphere) global emission inventory
452 gave a much higher biogenic emission of isoprene (15.72 Tg C yr^{-1}) and monoterpenes
453 (4.46 Tg C yr^{-1}) for the year 1990 based on a detailed multi-layer vegetation model
454 (Olivier et al., 2003; Granier et al., 2005). Global BVOC emissions are also computed
455 using the LPJ-GUESS (General Ecosystem Simulator-Emission) ecosystem model

456 coupled with a process-based emission algorithms, which gave an annual emission of
457 16.43 Tg C for isoprene and 1.84 Tg C for monoterpenes in 2006 (Arneth et al., 2007;
458 Schurgers et al., 2009).

459 **3.7.2 Comparisons with BVOC flux measurements**

460 By far, in China there are little intensive measurements of BVOC emission flux in
461 2006 due to their large spatial and temporal variability, as well as difficulty in
462 techniques of large-scale measurements. Hence, we just compared our estimated results
463 with limited data based on canopy-scale measurements from past references (Bai et al.,
464 2004; Baker et al., 2005; Geron et al., 2006; Gao et al., 2011).

465 Many measurements focused on BVOC emissions in Xishuangbanna, Yunnan
466 Province (21 °55'25"N, 101 °16'5"E) (Bai et al., 2004; Baker et al., 2005; Geron et al.,
467 2006). In July, 2002, Baker et al. (2005) measured the average emission of isoprene
468 during the daytime to be 1 mg C m^{-2} h^{-1}, which is close to our estimated average value
469 of 1.03 mg C m^{-2} h^{-1}. But the estimated flux of monoterpenes (0.3 mg C m^{-2} h^{-1}) was
470 much lower than the measured value (2 mg C m^{-2} h^{-1}). The measurement values given
471 by Geron et al. (2006) and Bai et al. (2004) also showed that the estimated values of
472 isoprene in this study agreed well with the measured values.

473 Compared to canopy-scale isoprene flux measurements conducted in July, 2008
474 for Guangdong (114 °45'44.7"E,22 °58'42.0"N), the estimated average daytime emission
475 flux (0.86 mg C m^{-2} h^{-1}) is higher than the average measured value of 0.2 mg C m^{-2} h^{-1}
476 approximately by a factor of 4.3.

4 Conclusions

Using MODIS-MM5-MEGAN, we estimated the total emission and spatial-temporal distributions of BVOC emissions from the terrestrial ecosystem in China for the year 2006. The annual total emission budget of BVOCs was roughly estimated to be 13.02 Tg C. Isoprene, with an annual emission of 9.39 Tg C, was the most abundant species (72%), followed by α-pinene (1.24 Tg C, 9.5%) and β-pinene (0.81 Tg C, 6.2%).

Spatially, isoprene emission centered in South China, with Yunnan contributing the largest (0.90 Tg C). While monoterpene emissions centered in Southeast China, where coniferous forests were extensively distributed and the top-ranking emitters were Guangxi and Yunnan (both 0.36 Tg C). In the main southern cities (Fujian, Guangxi, Hainan, Hunan, Jiangxi, and Yunnan), Shaanxi and Inner Mongolia, the high vegetation cover fractions resulted in that BVOC emissions predominated over anthropogenic NMVOC emissions.

Temporally, the seasonal and diurnal cycles of solar radiation and temperature as well as plant growth jointly led to strong variations in BVOC emissions. Generally, BVOC emission rates peaked in July, with daily maximum values occurring at about 13:00~14:00 (BJT).

Comparisons with past studies showed that, the dramatic land cover change and modified algorithms may be responsible for the great variations of estimated BVOC between studies. And intensive field measurements are needed for further evaluation and improvements of BVOC estimations in China.

The BVOC emission estimations presented in this study initiated an attempt to provide a systematic and real-time update of high-resolution BVOC emissions in China. On the basis of this study, we will further investigate the role of BVOCs in SOA formation and global climate change.

References

Arneth, A., Miller, P. A., Scholze, M., Hickler, T., Schurgers, G., Smith, B., and Prentice, I. C.: CO_2 inhibition of global terrestrial isoprene emissions: Potential implications for atmospheric chemistry, Geophys Res Lett, 34, Artn L18813. Doi 10.1029/2007gl030615, 2007.

Arneth, A., Monson, R. K., Schurgers, G., Niinemets, U., and Palmer, P. I.: Why are estimates of global terrestrial isoprene emissions so similar (and why is this not so for monoterpenes)?, Atmos Chem Phys, 8, 4605-4620, 2008.

Ashworth, K., Wild, O., and Hewitt, C. N.: Sensitivity of isoprene emissions estimated using MEGAN to the time resolution of input climate data, Atmos Chem Phys, 10, 1193-1201, 2010.

Atkinson, B. W.: Numerical modelling of urban heat-island intensity, Bound-Lay Meteorol, 109, 285-310, 2003.

Atkinson, R., and Arey, J.: Gas-phase tropospheric chemistry of biogenic volatile organic compounds: a review, Atmos Environ, 37, S197-S219, Doi 10.1016/S1352-2310(03)00391-1, 2003.

Bai, J., Baker, B., Johnson, C., Li, Q., Wang, Y., Zhao, C., Klinger, L., Guenther, A., and Greenberg, J.: Observational studies on volatile organic compounds of the tropical forest in Xishuangbanna, China Environmental Science, 24, 142-146, 2004.

Baker, B., Bai, J. H., Johnson, C., Cai, Z. T., Li, Q. J., Wang, Y. F., Guenther, A., Greenberg, J., Klinger, L., Geron, C., and Rasmussen, R.: Wet and dry season ecosystem level fluxes of isoprene and monoterpenes from a southeast Asian secondary forest and rubber tree plantation, Atmos Environ, 39, 381-390, DOI 10.1016/j.atmosenv.2004.07.033, 2005.

Benjamin, M. T., Sudol, M., Vorsatz, D., and Winer, A. M.: A spatially and temporally resolved biogenic hydrocarbon emissions inventory for the California South Coast Air Basin, Atmos Environ, 31, 3087-3100, 1997.

Benkovitz, C. M., Schwartz, S. E., Jensen, M. P., Miller, M. A., Easter, R. C., and Bates, T. S.: Modeling atmospheric sulfur over the Northern Hemisphere during the Aerosol Characterization Experiment 2 experimental period, J Geophys Res-Atmos, 109, Artn D22207. Doi 10.1029/2004jd004939, 2004.

Chen, F., and Dudhia, J.: Coupling an advanced land surface-hydrology model with the Penn State-NCAR MM5 modeling system. Part I: Model implementation and sensitivity, Mon Weather Rev, 129, 569-585, 2001.

Crawford, T. M., Stensrud, D. J., Mora, F., Merchant, J. W., and Wetzel, P. J.: Value of incorporating satellite-derived land cover data in MM5/PLACE for simulating surface temperatures, J Hydrometeorol, 2, 453-468, 2001.

de Foy, B., Molina, L. T., and Molina, M. J.: Satellite-derived land surface parameters for mesoscale modelling of the Mexico City basin, Atmos Chem Phys, 6, 1315-1330, 2006.

Gao, X., Zhang, H., Cai, X., Song, Y., and Kang, L.: VOCs fluxes analysis based on micrometeorological methods over Litchi Plantation in the Pearl River Delta, China, Acta Scientiarum Naturalium Universitatis Pekinensis, 47, 916-922, 2011.

Garrigues, S., Lacaze, R., Baret, F., Morisette, J. T., Weiss, M., Nickeson, J. E., Fernandes, R., Plummer, S., Shabanov, N. V., Myneni, R. B., Knyazikhin, Y., and Yang, W.: Validation and intercomparison of global Leaf Area Index products derived from remote sensing data, J Geophys Res-Biogeo, 113, Artn G02028. Doi 10.1029/2007jg000635, 2008.

Ge, J. J., Qi, J. G., and Lofgren, B.: Use of vegetation properties from EOS observations for land-climate modeling in East Africa, J Geophys Res-Atmos, 113, Artn D15101. Doi 10.1029/2007jd009628, 2008.

Geron, C., Owen, S., Guenther, A., Greenberg, J., Rasmussen, R., Bai, J. H., Li, Q. J., and Baker, B.: Volatile organic compounds from vegetation in southern Yunnan Province, China: Emission rates and some potential regional implications, Atmos Environ, 40, 1759-1773, DOI 10.1016/j.atmosenv.2005.11.022, 2006.

Goldstein, A. H., and Galbally, I. E.: Known and unexplored organic constituents in the Earth's atmosphere, Geochim Cosmochim Ac, 73, A449-A449, 2009.

Granier, C., Lamarque, J. F., Mieville, A., Muller, J. F., Olivier, J., Orlando, J., Peters, J., Petron, G., Tyndall, S., and Wallens, S.: POET, a database of surface emissions of zone precursors, 2005.

Griffin, R. J., Cocker, D. R., Flagan, R. C., and Seinfeld, J. H.: Organic aerosol formation from the oxidation of biogenic hydrocarbons, J Geophys Res-Atmos, 104, 3555-3567, 1999.

Guenther, A., Hewitt, C. N., Erickson, D., Fall, R., Geron, C., Graedel, T., Harley, P., Klinger, L., Lerdau, M., Mckay, W. A., Pierce, T., Scholes, B., Steinbrecher, R., Tallamraju, R., Taylor, J., and Zimmerman, P.: A Global-Model of Natural Volatile Organic-Compound Emissions, J Geophys Res-Atmos, 100, 8873-8892, 1995.

Guenther, A., Archer, S., Greenberg, J., Harley, P., Helmig, D., Klinger, L., Vierling, L., Wildermuth, M., Zimmerman, P., and Zitzer, S.: Biogenic hydrocarbon emissions and landcover/climate change in a subtropical savanna, Phys Chem Earth Pt B, 24, 659-667, 1999.

Guenther, A., Karl, T., Harley, P., Wiedinmyer, C., Palmer, P. I., and Geron, C.: Estimates of global terrestrial isoprene emissions using MEGAN (Model of Emissions of Gases and Aerosols from Nature), Atmos Chem Phys, 6, 3181-3210, 2006.

Gutman, G., and Ignatov, A.: The derivation of the green vegetation fraction from NOAA/AVHRR data for use in numerical weather prediction models, Int J Remote Sens, 19, 1533-1543, 1998.

Hallquist, M., Wenger, J. C., Baltensperger, U., Rudich, Y., Simpson, D., Claeys, M., Dommen, J., Donahue, N. M., George, C., Goldstein, A. H., Hamilton, J. F., Herrmann, H., Hoffmann, T., Iinuma, Y., Jang, M., Jenkin, M. E., Jimenez, J. L., Kiendler-Scharr, A., Maenhaut, W., McFiggans, G., Mentel, T. F., Monod, A., Prevot, A. S. H., Seinfeld, J. H., Surratt, J. D., Szmigielski, R., and Wildt, J.: The formation, properties and impact of secondary organic aerosol: current and emerging issues, Atmos Chem Phys, 9, 5155-5236, 2009.

Jakubauskas, M., Kindscher, K., Fraser, A., Debinski, D., and Price, K. P.: Close-range remote sensing of aquatic macrophyte vegetation cover, Int J Remote Sens, 21, 3533-3538, 2000.

Jiang, L., Kogan, F. N., Guo, W., Tarpley, J. D., Mitchell, K. E., Ek, M. B., Tian, Y. H., Zheng, W. Z., Zou, C. Z., and Ramsay, B. H.: Real-time weekly global green vegetation fraction derived from advanced very high resolution radiometer-based NOAA operational global vegetation index (GVI) system, J Geophys Res-Atmos, 115, Artn D11114. Doi 10.1029/2009jd013204, 2010.

Justice, C. O., Townshend, J. R. G., Vermote, E. F., Masuoka, E., Wolfe, R. E., Saleous, N., Roy, D. P., and Morisette, J. T.: An overview of MODIS Land data processing and product status, Remote Sens Environ, 83, 3-15, 2002.

Kanakidou, M., Seinfeld, J. H., Pandis, S. N., Barnes, I., Dentener, F. J., Facchini, M. C., Van Dingenen, R., Ervens, B., Nenes, A., Nielsen, C. J., Swietlicki, E., Putaud, J. P., Balkanski, Y., Fuzzi, S., Horth, J., Moortgat, G. K., Winterhalter, R., Myhre, C. E. L., Tsigaridis, K., Vignati, E., Stephanou, E. G., and Wilson, J.: Organic aerosol and global climate modelling: a review, Atmos Chem Phys, 5, 1053-1123, 2005.

Karl, M., Guenther, A., Koble, R., Leip, A., and Seufert, G.: A new European plant-specific emission inventory of biogenic volatile organic compounds for use in atmospheric transport models, Biogeosciences, 6, 1059-1087, 2009.

Kesselmeier, J., and Staudt, M.: Biogenic volatile organic compounds (VOC): An overview on emission, physiology and ecology, Journal of Atmospheric Chemistry, 33, 23-88, 1999.

Kesselmeier, J., Ciccioli, P., Kuhn, U., Stefani, P., Biesenthal, T., Rottenberger, S., Wolf, A., Vitullo, M., Valentini, R., Nobre, A., Kabat, P., and Andreae, M. O.: Volatile organic compound emissions in relation to plant carbon fixation and the terrestrial carbon budget, Global Biogeochem Cy, 16, Artn 1126. Doi 10.1029/2001gb001813, 2002.

Klinger, L. F., Li, Q. J., Guenther, A. B., Greenberg, J. P., Baker, B., and Bai, J. H.: Assessment of volatile organic compound emissions from ecosystems of China, J

Geophys Res-Atmos, 107, Artn 4603. Doi 10.1029/2001jd001076, 2002.

Kurkowski, N. P., Stensrud, D. J., and Baldwin, M. E.: Assessment of implementing satellite-derived land cover data in the Eta model, Weather Forecast, 18, 404-416, 2003.

Kuzma, J., Nemecekmarshall, M., Pollock, W. H., and Fall, R.: Bacteria Produce the Volatile Hydrocarbon Isoprene, Curr Microbiol, 30, 97-103, 1995.

Lane, T. E., and Pandis, S. N.: Predicted secondary organic aerosol concentrations from the oxidation of isoprene in the Eastern United States, Environ Sci Technol, 41, 3984-3990, Doi 10.1021/Es061312q, 2007.

Leung, D. Y. C., Wong, P., Cheung, B. K. H., and Guenther, A.: Improved land cover and emission factors for modeling biogenic volatile organic compounds emissions from Hong Kong, Atmos Environ, 44, 1456-1468, DOI 10.1016/j.atmosenv.2010.01.012, 2010.

Liao, H., Henze, D. K., Seinfeld, J. H., Wu, S. L., and Mickley, L. J.: Biogenic secondary organic aerosol over the United States: Comparison of climatological simulations with observations, J Geophys Res-Atmos, 112, Artn D06201. Doi 10.1029/2006jd007813, 2007.

McKay, W. A., Turner, M. F., Jones, B. M. R., and Halliwell, C. M.: Emissions of hydrocarbons from marine phytoplankton - Some results from controlled laboratory experiments, Atmos Environ, 30, 2583-2593, 1996.

Meng, X. H., Lu, S. H., Zhang, T. T., Guo, J. X., Gao, Y. H., Bao, Y., Wen, L. J., Luo, S. Q., and Liu, Y. P.: Numerical simulations of the atmospheric and land conditions over the Jinta oasis in northwestern China with satellite-derived land surface parameters, J Geophys Res-Atmos, 114, Artn D06114. Doi 10.1029/2008jd010360, 2009.

Molders, N.: On the uncertainty in mesoscale modeling caused by surface parameters, Meteorol Atmos Phys, 76, 119-141, 2001.

Monks, P. S., Granier, C., Fuzzi, S., Stohl, A., Williams, M. L., Akimoto, H., Amann, M., Baklanov, A., Baltensperger, U., Bey, I., Blake, N., Blake, R. S., Carslaw, K., Cooper, O. R., Dentener, F., Fowler, D., Fragkou, E., Frost, G. J., Generoso, S., Ginoux, P., Grewe, V., Guenther, A., Hansson, H. C., Henne, S., Hjorth, J., Hofzumahaus, A., Huntrieser, H., Isaksen, I. S. A., Jenkin, M. E., Kaiser, J., Kanakidou, M., Klimont, Z., Kulmala, M., Laj, P., Lawrence, M. G., Lee, J. D., Liousse, C., Maione, M., McFiggans, G., Metzger, A., Mieville, A., Moussiopoulos, N., Orlando, J. J., O'Dowd, C. D., Palmer, P. I., Parrish, D. D., Petzold, A., Platt, U., Poschl, U., Prevot, A. S. H., Reeves, C. E., Reimann, S., Rudich, Y., Sellegri, K., Steinbrecher, R., Simpson, D., ten Brink, H., Theloke, J., van der Werf, G. R., Vautard, R., Vestreng, V., Vlachokostas, C., and von Glasow, R.: Atmospheric composition change - global and regional air quality, Atmos Environ, 43, 5268-5350, 2009.

Olivier, J., Peters, J., Granier, C., Petron, G., Muller, J. F., and Wallens, S.: Present and future surface emissions of atmospheric compounds, POET report #2, EU project EVK2-1999-00011, 2003.

Pacifico, F., Harrison, S. P., Jones, C. D., and Sitch, S.: Isoprene emissions and climate, Atmos Environ, 43, 6121-6135, DOI 10.1016/j.atmosenv.2009.09.002, 2009.

Perraud, V., Bruns, E. A., Ezell, M. J., Johnson, S. N., Yu, Y., Alexander, M. L., Zelenyuk, A., Imre, D., and Pitts, B. J. F.: Contribution from O_3 chemistry to secondary organic aerosol formation during the NO_3 radical-initiated oxidation of alpha-pinene, Abstracts of Papers of the American Chemical Society, 241, 2011.

Pielke, R. A., Marland, G., Betts, R. A., Chase, T. N., Eastman, J. L., Niles, J. O., Niyogi, D. D. S., and Running, S. W.: The influence of land-use change and landscape dynamics on the climate system: relevance to climate-change policy beyond the radiative effect of greenhouse gases, Philos T Roy Soc A, 360, 1705-1719, DOI 10.1098/rsta.2002.1027, 2002.

Purevdorj, T., Tateishi, R., Ishiyama, T., and Honda, Y.: Relationships between percent vegetation cover and vegetation indices, Int J Remote Sens, 19, 3519-3535, 1998.

Ryerson, T. B., Trainer, M., Holloway, J. S., Parrish, D. D., Huey, L. G., Sueper, D. T., Frost, G. J., Donnelly, S. G., Schauffler, S., Atlas, E. L., Kuster, W. C., Goldan, P. D., Hubler, G., Meagher, J. F., and Fehsenfeld, F. C.: Observations of ozone formation in power plant plumes and implications for ozone control strategies, Science, 292, 719-723, 2001.

Sakulyanontvittaya, T., Duhl, T., Wiedinmyer, C., Helmig, D., Matsunaga, S., Potosnak, M., Milford, J., and Guenther, A.: Monoterpene and sesquiterpene emission estimates for the United States, Environ Sci Technol, 42, 1623-1629, Doi 10.1021/Es702274e, 2008.

Schell, B., Ackermann, I. J., Hass, H., Binkowski, F. S., and Ebel, A.: Modeling the formation of secondary organic aerosol within a comprehensive air quality model system, J Geophys Res-Atmos, 106, 28275-28293, 2001.

Schurgers, G., Arneth, A., Holzinger, R., and Goldstein, A. H.: Process-based modelling of biogenic monoterpene emissions combining production and release from storage, Atmos Chem Phys, 9, 3409-3423, 2009.

Streets, D. G., Bond, T. C., Carmichael, G. R., Fernandes, S. D., Fu, Q., He, D., Klimont, Z., Nelson, S. M., Tsai, N. Y., Wang, M. Q., Woo, J. H., and Yarber, K. F.: An inventory of gaseous and primary aerosol emissions in Asia in the year 2000, J Geophys Res-Atmos, 108, Artn 8809. Doi 10.1029/2002jd003093, 2003.

Szidat, S., Jenk, T. M., Synal, H. A., Kalberer, M., Wacker, L., Hajdas, I., Kasper-Giebl, A., and Baltensperger, U.: Contributions of fossil fuel, biomass-burning, and biogenic emissions to carbonaceous aerosols in Zurich as traced by (14)C, J Geophys Res-Atmos, 111, Artn D07206. Doi 10.1029/2005jd006590, 2006.

699 Tian, Y., Dickinson, R. E., Zhou, L., Myneni, R. B., Friedl, M., Schaaf, C. B., Carroll,
700 M., and Gao, F.: Land boundary conditions from MODIS data and consequences
701 for the albedo of a climate model, Geophys Res Lett, 31, Artn L05504. Doi
702 10.1029/2003gl019104, 2004.

703 Tie, X. X., Li, G. H., Ying, Z. M., Guenther, A., and Madronich, S.: Biogenic emissions
704 of isoprenoids and NO in China and comparison to anthropogenic emissions, Sci
705 Total Environ, 371, 238-251, DOI 10.1016/j.scitotenv.2006.06.025, 2006.

706 Wang, Q. G., Han, Z. W., Wang, T. J., and Higano, Y.: An estimate of biogenic
707 emissions of volatile organic compounds during summertime in China, Environ
708 Sci Pollut R, 14, 69-75, DOI 10.1065/espr2007.01.376, 2007.

709 Wang, X. M., Situ, S. P., Guenther, A., Chen, F., Wu, Z. Y., Xia, B. C., and Wang, T. J.:
710 Spatiotemporal variability of biogenic terpenoid emissions in Pearl River Delta,
711 China, with high-resolution land-cover and meteorological data, Tellus B, 63,
712 241-254, DOI 10.1111/j.1600-0889.2010.00523.x, 2011.

713 Wang, Z. H., Bai, Y. H., and Zhang, S. Y.: A biogenic volatile organic compounds
714 emission inventory for Beijing, Atmos Environ, 37, 3771-3782, Doi
715 10.1016/S1352-2310(03)00462-X, 2003.

716 Warneke, C., de Gouw, J. A., Del Negro, L., Brioude, J., McKeen, S., Stark, H., Kuster,
717 W. C., Goldan, P. D., Trainer, M., Fehsenfeld, F. C., Wiedinmyer, C., Guenther, A.
718 B., Hansel, A., Wisthaler, A., Atlas, E., Holloway, J. S., Ryerson, T. B., Peischl, J.,
719 Huey, L. G., and Hanks, A. T. C.: Biogenic emission measurement and inventories
720 determination of biogenic emissions in the eastern United States and Texas and
721 comparison with biogenic emission inventories, J Geophys Res-Atmos, 115, Artn
722 D00f18. Doi 10.1029/2009jd012445, 2010.

723 Went, F. W.: Blue Hazes in the Atmosphere, Nature, 187, 641-643, 1960.

724 Wittich, K. P., and Hansing, O.: Area-Averaged Vegetative Cover Fraction Estimated
725 from Satellite Data, Int J Biometeorol, 38, 209-215, 1995.

726 Yucel, I.: Effects of implementing MODIS land cover and albedo in MM5 at two
727 contrasting US regions, J Hydrometeorol, 7, 1043-1060, 2006.

728 Zemankova, K., and Brechler, J.: Emissions of biogenic VOC from forest ecosystems
729 in central Europe: Estimation and comparison with anthropogenic emission
730 inventory, Environmental Pollution, 158, 462-469, DOI
731 10.1016/j.envpol.2009.08.032, 2010.

732 Zhang, Q., Streets, D. G., Carmichael, G. R., He, K. B., Huo, H., Kannari, A., Klimont,
733 Z., Park, I. S., Reddy, S., Fu, J. S., Chen, D., Duan, L., Lei, Y., Wang, L. T., and
734 Yao, Z. L.: Asian emissions in 2006 for the NASA INTEX-B mission, Atmos
735 Chem Phys, 9, 5131-5153, 2009.

736 Zheng, J. Y., Zheng, Z. Y., Yu, Y. F., and Zhong, L. J.: Temporal, spatial
737 characteristics and uncertainty of biogenic VOC emissions in the Pearl River

738 Delta region, China, Atmos Environ, 44, 1960-1969, DOI
739 10.1016/j.atmosenv.2010.03.001, 2010.

740

741

742

743 Table 1 The mapping of land-use classes of MODIS to USGS classifications

MODIS		USGS	
Category	Land-use Description	Category	Land-use Description
0	Water	16	Water bodies
1	Evergreen Coniferous Forest	14	Evergreen Coniferous forest
2	Evergreen Broadleaf Forest	13	Evergreen Broadleaf forest
3	Deciduous Coniferous Forest	12	Deciduous Coniferous forest
4	Deciduous Broadleaf Forest	11	Deciduous Broadleaf forest
5	Mixed Forest	15	Mixed Forest
6	Closed Shrubland	8	Shrubland
7	Open Shrubland	9	Mixed Shrubland/Grass
8	Woody savanna	10	Savanna
9	Savanna	10	Savanna
10	Grassland	7	Grassland
11	Permanent wetland	17	Herb. Wetland
12	Cropland	5	Crop/Grass Mosaic
13	Urban and Built-up	1	Urban
14	Cropland/Natural Vegetation Mosaic	6	Crop/Wood Mosaic
15	Snow and Ice	24	Snow or Ice
16	Barren or Sparsely Vegetated	19	Barren or Sparsely Vegetated
254	Unclassified	25	No Data

744 Table 2 Statistical analyses of air temperature at 2 m (T2) and solar shortwave radiation

745 (SWDOWN) for four seasons

Variable	Season	MeanObs [a]	MeanSim [a]	R [a]	MB [a]	ME [a]	RMSE [a]	MNB [a]	MNE [a]
T2 (℃)	Spring	12.97	12.41	0.95	-0.56	2.35	3.22	-0.05	0.16
	Summer	23.62	24.29	0.91	0.67	2.33	3.09	0.03	0.12
	Autumn	13.66	13.10	0.96	-0.56	2.15	2.89	-0.03	0.13
	Winter	-0.12	-0.75	0.95	-0.62	2.62	3.52	-0.05	0.02
	year	12.66	12.40	0.97	-0.26	2.36	3.19	-0.02	0.11
SWDOWN ($W\ m^{-2}$)	Spring	196.95	220.58	0.59	23.63	65.88	90.44	0.52	0.74
	Summer	218.80	246.20	0.50	27.40	77.49	101.27	0.38	0.61
	Autumn	144.31	156.34	0.62	12.03	48.28	67.92	0.30	0.56
	Winter	102.95	112.77	0.57	9.81	40.29	58.32	0.61	0.88
	year	166.13	184.41	0.67	18.28	58.10	81.45	0.45	0.70

746 [a] MeanObs: Mean Observed value, MeanSim: Mean Simulated Value, R: Correlation

747 coefficient, MB: Mean Bias, ME: Mean Error, RMSE: Root Mean Square Error, MNB:

748 Mean Normalized Bias, MNE: Mean Normalized Error.

749 Table 3 Monthly emission budgets of BVOCs in China estimated by this study (Tg C)

season	ISO [b]	MT [b]								Total
		APIN	BPIN	3-CAR	OCIM	LIMO	SABI	MYRC	Total	
March	0.17	0.03	0.02	0.02	0.01	0.01	0.005	0.003	0.10	0.27
April	0.44	0.07	0.05	0.04	0.02	0.01	0.01	0.01	0.21	0.65
May	0.86	0.12	0.08	0.07	0.03	0.03	0.02	0.01	0.36	1.22
Spring [a]	1.47	0.22	0.15	0.13	0.06	0.05	0.035	0.023	0.67	2.14
June	1.44	0.18	0.12	0.10	0.05	0.04	0.03	0.02	0.54	1.98
July	2.42	0.26	0.17	0.14	0.07	0.06	0.04	0.02	0.76	3.18
August	2.41	0.26	0.17	0.13	0.07	0.06	0.04	0.02	0.75	3.16
Summer [a]	6.27	0.70	0.46	0.37	0.19	0.16	0.11	0.06	2.05	8.32
September	0.89	0.14	0.09	0.08	0.03	0.03	0.02	0.01	0.40	1.29
October	0.42	0.08	0.06	0.05	0.02	0.02	0.01	0.01	0.25	0.67
November	0.16	0.04	0.02	0.02	0.01	0.01	0.005	0.003	0.11	0.27
Autumn [a]	1.47	0.26	0.17	0.15	0.06	0.06	0.035	0.023	0.76	2.23
December	0.06	0.02	0.01	0.01	0.004	0.005	0.003	0.002	0.05	0.11
January	0.05	0.02	0.01	0.01	0.004	0.004	0.003	0.002	0.05	0.10
February	0.07	0.02	0.01	0.01	0.004	0.004	0.003	0.001	0.05	0.12
Winter [a]	0.18	0.06	0.03	0.03	0.01	0.01	0.01	0.005	0.15	0.33
Annual	9.39	1.24	0.81	0.68	0.32	0.28	0.19	0.11	3.63	13.02

750 [a] Spring: March, April and May; Summer: June, July and August; Autumn: September,
751 October and November; Winter: December, January and February.
752 [b] ISO, isoprene; MT, monoterpene; APIN, α-pinene; BPIN, β-pinene; 3-CAR, 3-carene;
753 OCIM, ocimene; LIMO, limonene; SABI, sabinene; MYRC, myrcene.
754
755
756
757
758

759 Table 4 Estimated BVOC emission budgets in this study and AVOC emission budgets
760 calculated by Zhang et al. (2009) by province (Tg C for BVOCs; Tg compound for
761 AVOCs and VOC)

762

Province	Isoprene	Monoterpene	AVOCs	VOC
Anhui	0.27	0.10	0.96	1.38
Beijing	0.03	0.004	0.50	0.54
Chongqing	0.22	0.06	0.34	0.66
Fujian	0.46	0.25	0.70	1.50
Gansu	0.15	0.035	0.30	0.51
Guangdong	0.46	0.27	1.78	2.61
Guangxi	0.66	0.36	0.64	1.80
Guizhou	0.29	0.14	0.48	0.97
Hainan	0.15	0.07	0.12	0.37
Hebei	0.15	0.04	1.52	1.74
Heilongjiang	0.53	0.19	0.77	1.59
Henan	0.18	0.06	1.29	1.56
Hong Kong [a]	0.77	0.52	0.11	0.11
Hubei	0.48	0.14	0.88	1.58
Hunan	0.75	0.30	0.64	1.83
Inner Mongolia	0.44	0.11	0.57	1.19
Jiangsu	0.08	0.03	1.79	1.91
Jiangxi	0.58	0.28	0.52	1.49
Jilin	0.22	0.07	0.51	0.84
Liaoning	0.12	0.04	0.97	1.15
Ningxia	0.02	0.00	0.13	0.15
Qinghai	0.08	0.01	0.07	0.17
Shaanxi	0.42	0.09	0.49	1.07
Shandong	0.07	0.035	2.09	2.21
Shanghai [a]	2.82	0.59	0.59	0.59
Shanxi	0.14	0.03	0.63	0.82
Sichuan	0.66	0.23	1.31	2.32
Taiwan	0.10	0.05	—	0.17
Tianjin [a]	5.12	1.83	0.38	0.39
Tibet	0.30	0.09	0.01	0.45
Xinjiang	0.15	0.03	0.39	0.59
Yunnan	0.90	0.36	0.51	1.94
Zhejiang	0.32	0.16	1.23	1.77
Total	9.39	3.63	23.25	38.01

763 [a] The unit of BVOCs in Hong Kong, Shanghai and Tianjin is Gg C.

764 Table 5 Comparisons of the estimated BVOC budgets (Tg C yr^{-1}) with previous studies

Region	Base year	resolution	Emission Budget			Reference
			ISO	MT	Total	
China	2006	12km×12km	9.39	3.63	13.02	This study
	2004	10km×10km	7.70	3.16	10.86	Tie et al. (2006)
	_	0.5°×0.5°	4.06	3.47	7.53	Klinger et al. (2002)
	_	0.5°×0.5°	15.00	4.30	19.3	Guenther et al. (1995)
	2000	0.5°×0.5°	10.01	2.53	12.54	Guenther et al. (2006) [a]
	1990	1°×1°	15.72	4.46	20.18	POET global inventory[a]
	2006	1°×1°	16.43	1.84	18.27	GUESS-ES [a]

765 [a] The regional emission data of Guenther et al. (2006), POET global emission inventory
766 and GUESS-ES were downloaded from the ECCAD (Emission of atmospheric
767 Compounds & Compilation of Ancillary Data) -GEIA (Global Emissions Inventory
768 Activity) database website (http://eccad.sedoo.fr/).

769 Table 6 Estimated BVOC emission budgets by different case studies (Tg C)

case [a]	Isoprene					Monoterpenes				
	Spring	Summer	Autumn	Winter	Year	Spring	Summer	Autumn	Winter	Year
This study	1.47	6.27	1.47	0.18	9.39	0.67	2.05	0.76	0.15	3.63
Tie et al. (2006)	2.00	5.05	0.47	0.18	7.7	0.81	1.78	0.41	0.16	3.16
Case 1	5.10	6.67	3.35	1.96	17.08	0.70	1.77	0.59	0.144	3.20
Case 2	3.60	4.76	2.21	1.17	11.74	0.51	1.30	0.46	0.12	2.39
Case 3	0.76	2.78	0.61	0.12	4.27	—	—	—	—	—

770 [a] Tie et al. (2006): WRF + EF/USGS + algorithms in Tie et al. (2006);
771 Case 1: MM5 + EF/MODIS + algorithms in Tie et al. (2006);
772 Case 2: MM5 + EF/USGS + algorithms in Tie et al. (2006);
773 Case 3: MM5 + EF/USGS + algorithms in this study.

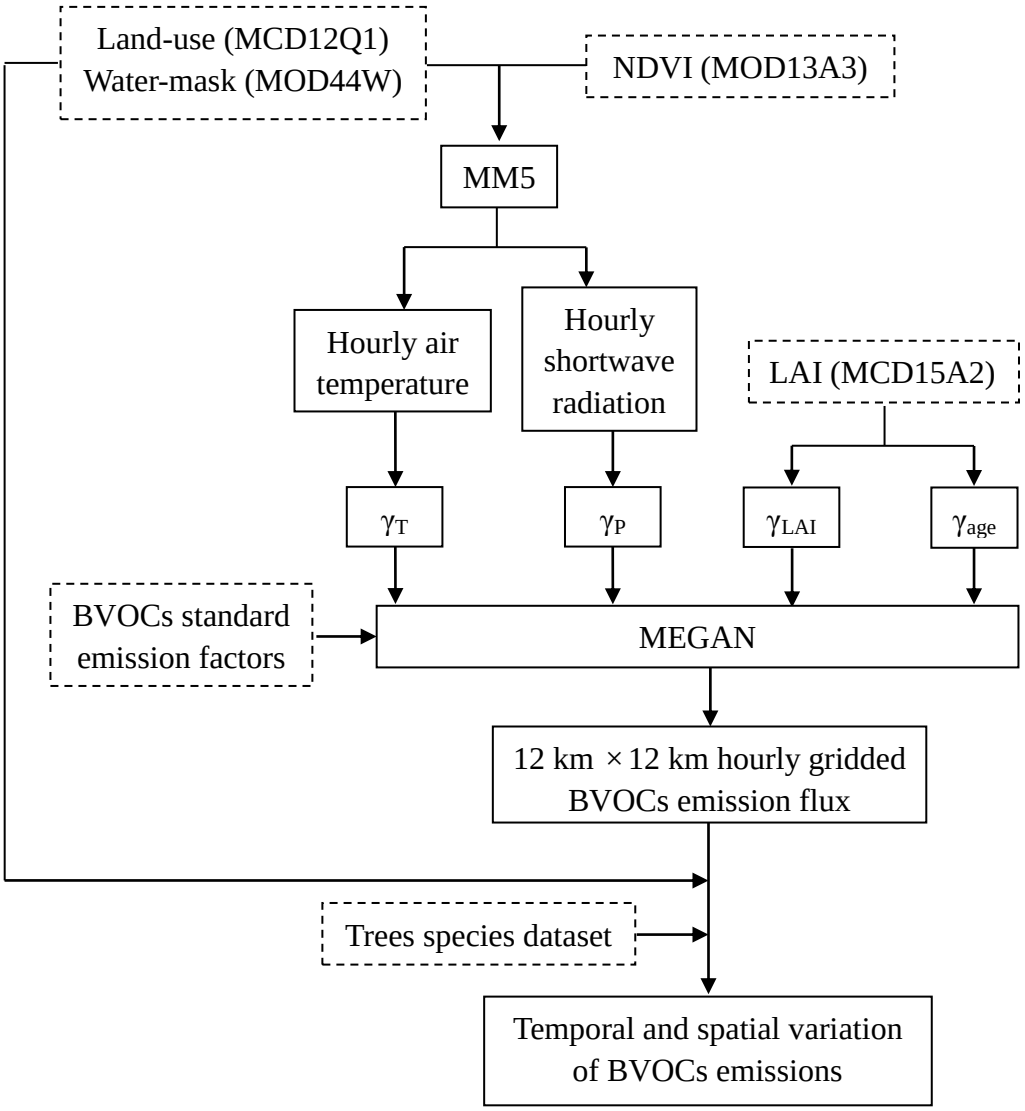

774

775 Fig. 1 Flowchart of the estimation of BVOC emissions, in which the dashed line box

776 representing the model input

777

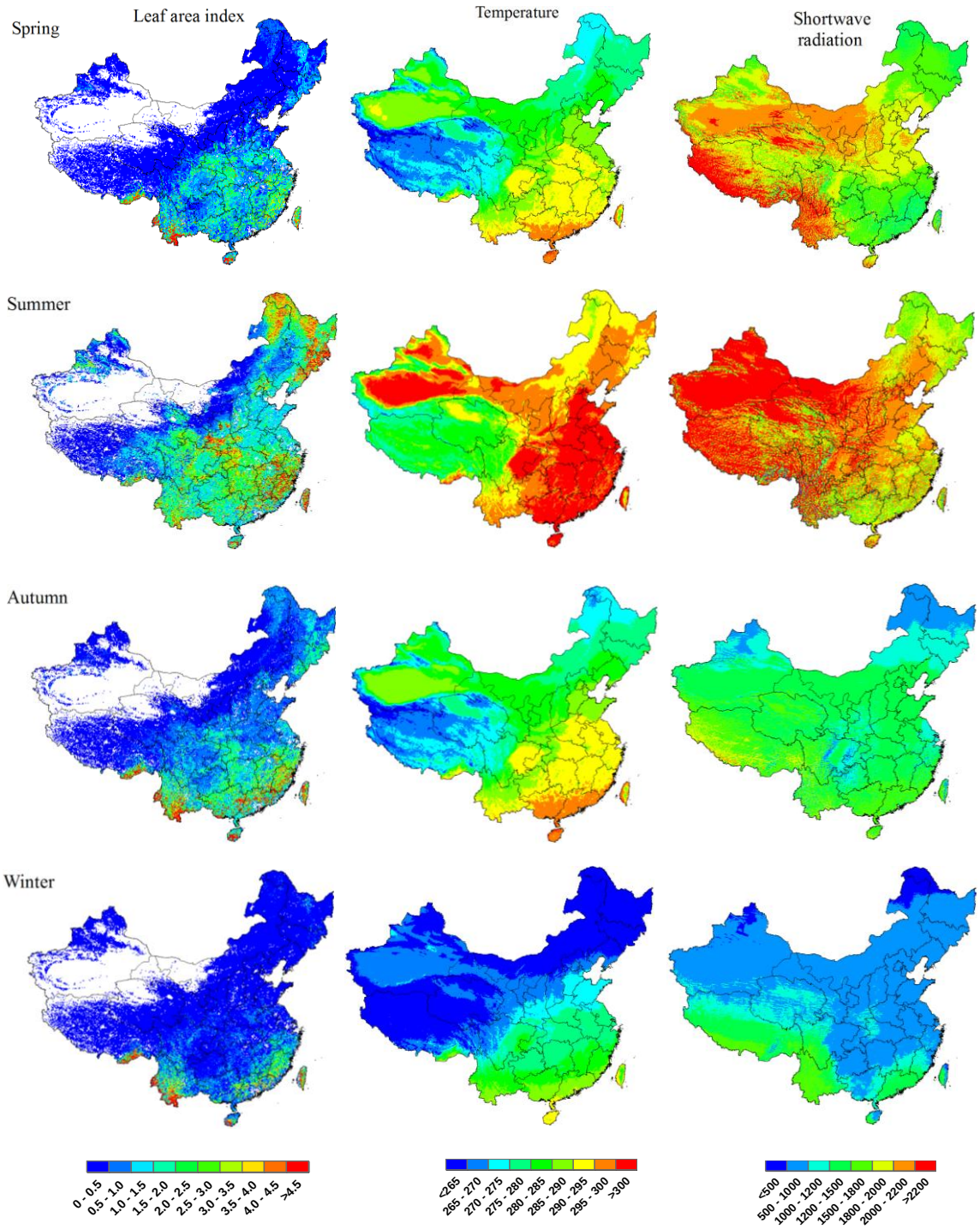

778 Fig. 2 Average seasonal LAI values for China derived from MODIS data (left panel),
779 simulated air temperature at 2 m (K) (middle panel) and total solar shortwave radiation
780 energy per season (MJ m^{-2}) (right panel)
781

782

783

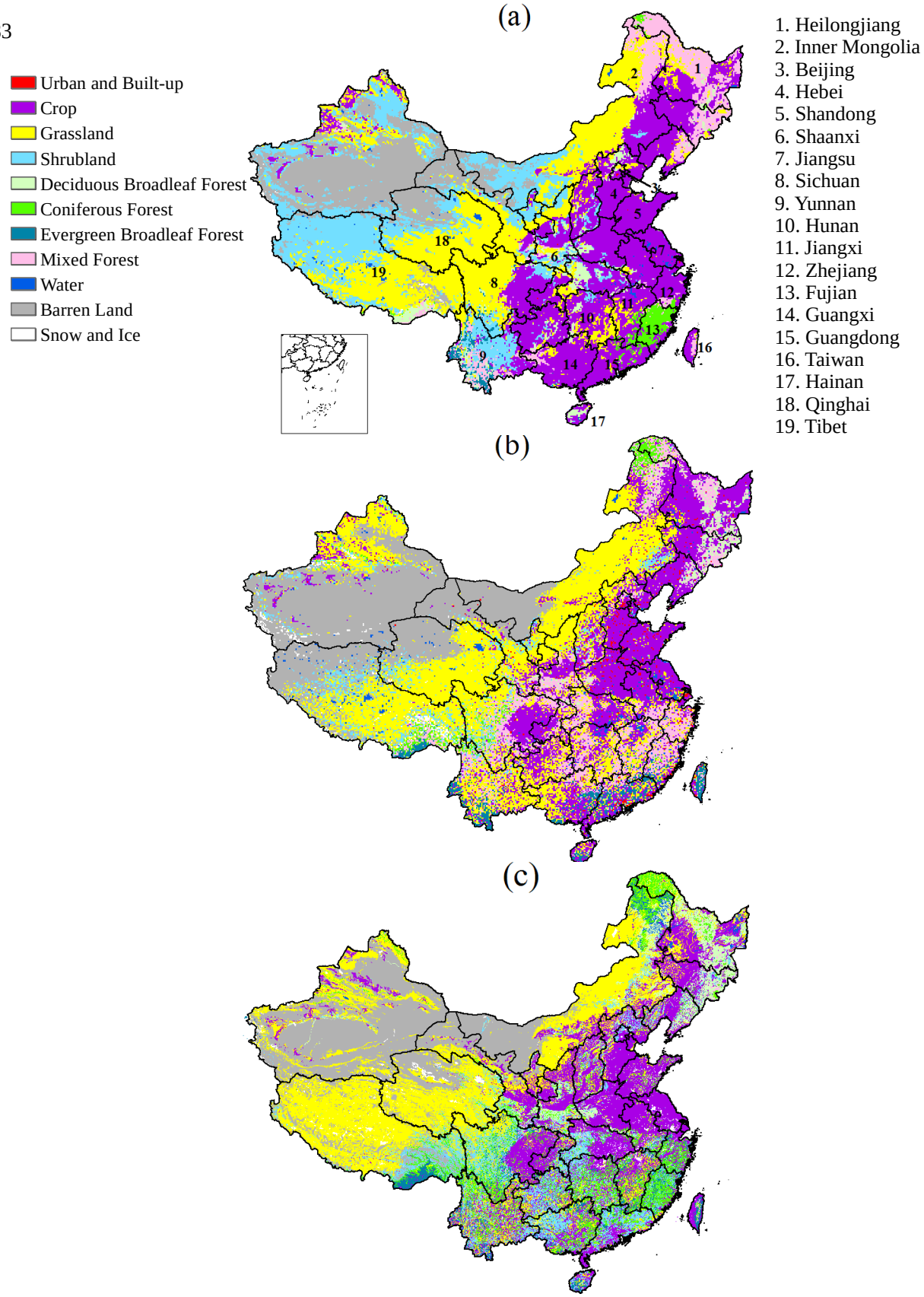

784 Fig. 3 Land-use maps for China derived from: (a) the default USGS data; (b) MODIS

785 observations; (c) tree species distribution data from the Plant Research Institute of the

Chinese Academy of Sciences (to avoid confusion, the location of the Nansha Islands was not marked in the figures below)

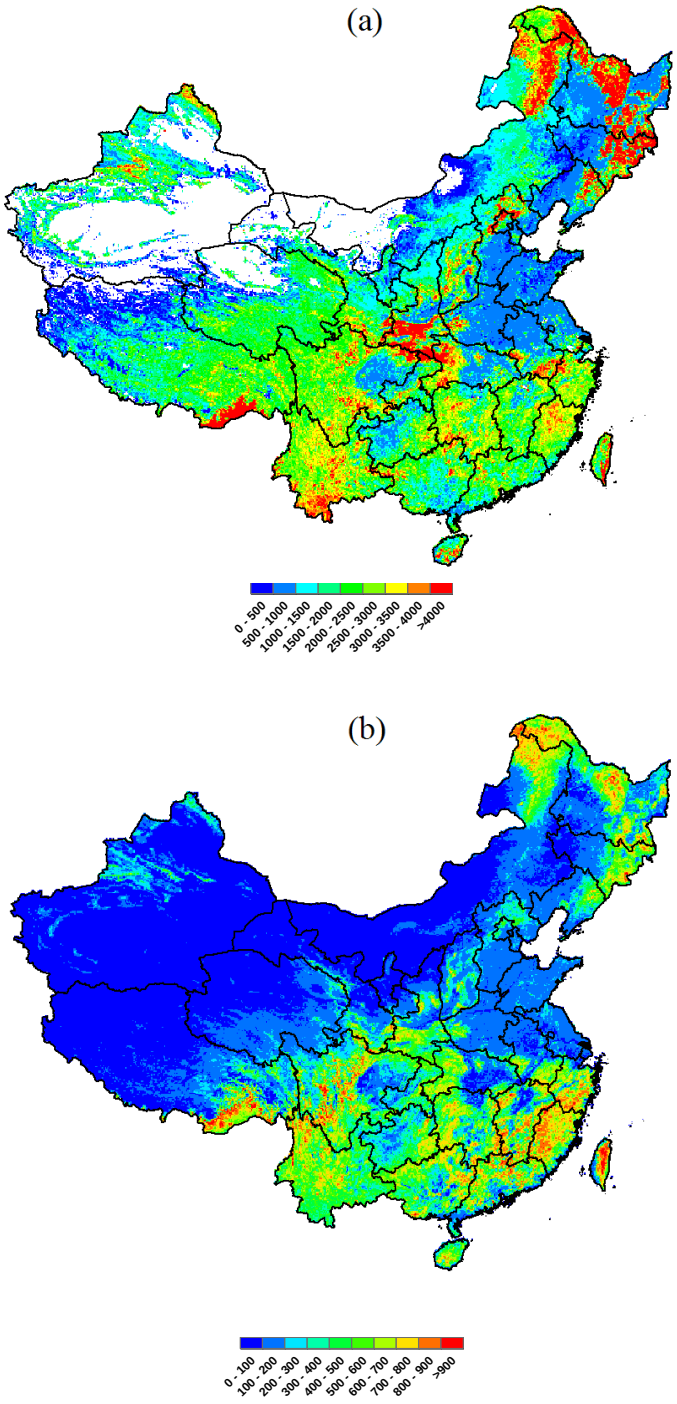

788

789

790

791

792 Fig. 4 Standard BVOC emission factors (g C km^{-2} h^{-1}) for China based on 1 km × 1 km

793 grid: (a) isoprene; (b) monoterpenes

794

795

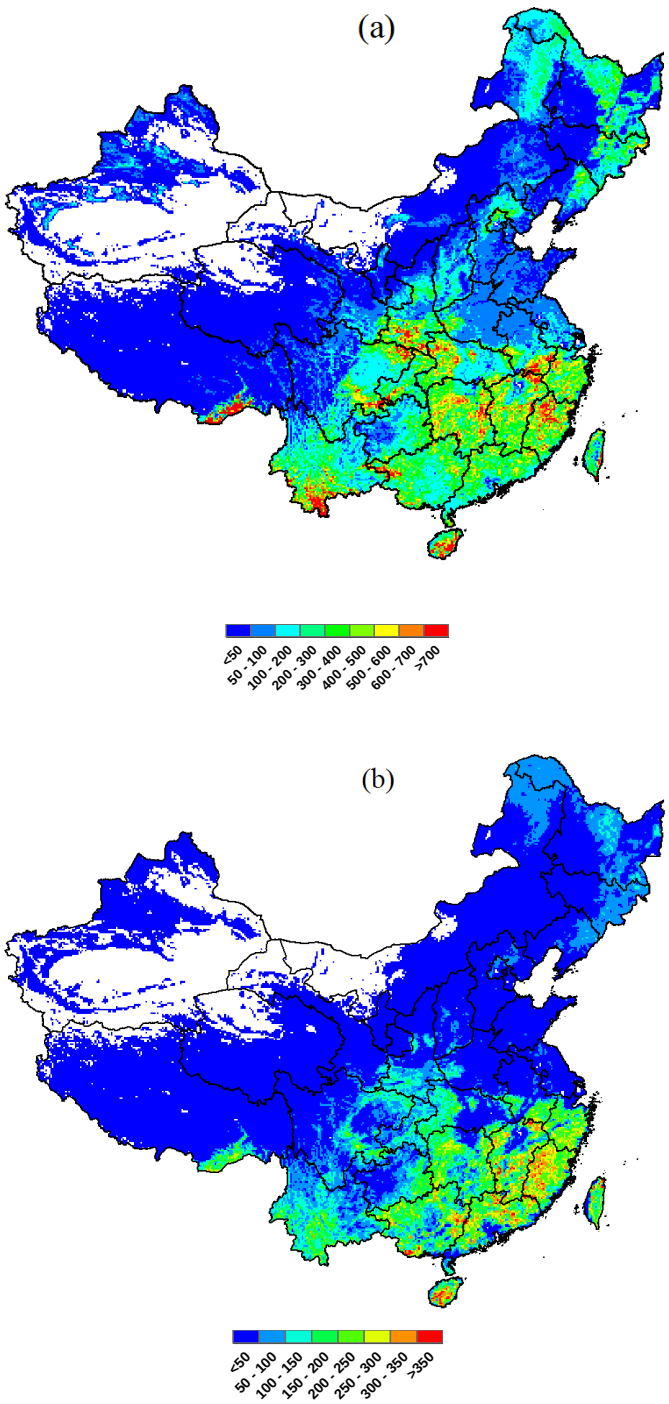

796

797

798

799

800 Fig. 5 Average (calculated) yearly biogenic emission fluxes of BVOCs (g C km^{-2} h^{-1})

801 for China in 2006: (a) isoprene; (b) monoterpenes

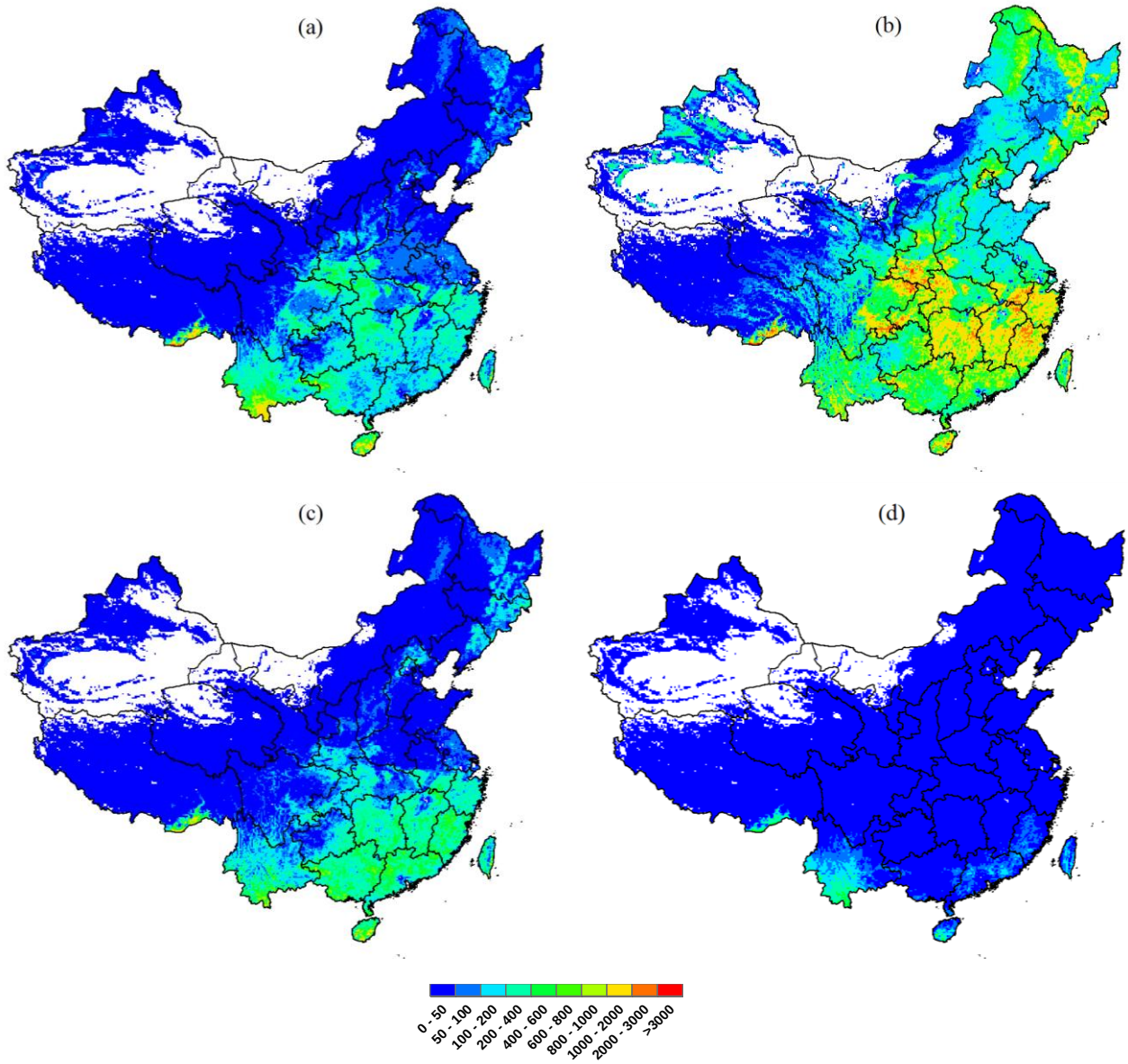

804

805

806 Fig. 6 Average (calculated) seasonal isoprene emission fluxes (g C km^{-2} h^{-1}): (a) spring;

807 (b) summer; (c) autumn; (d) winter

808

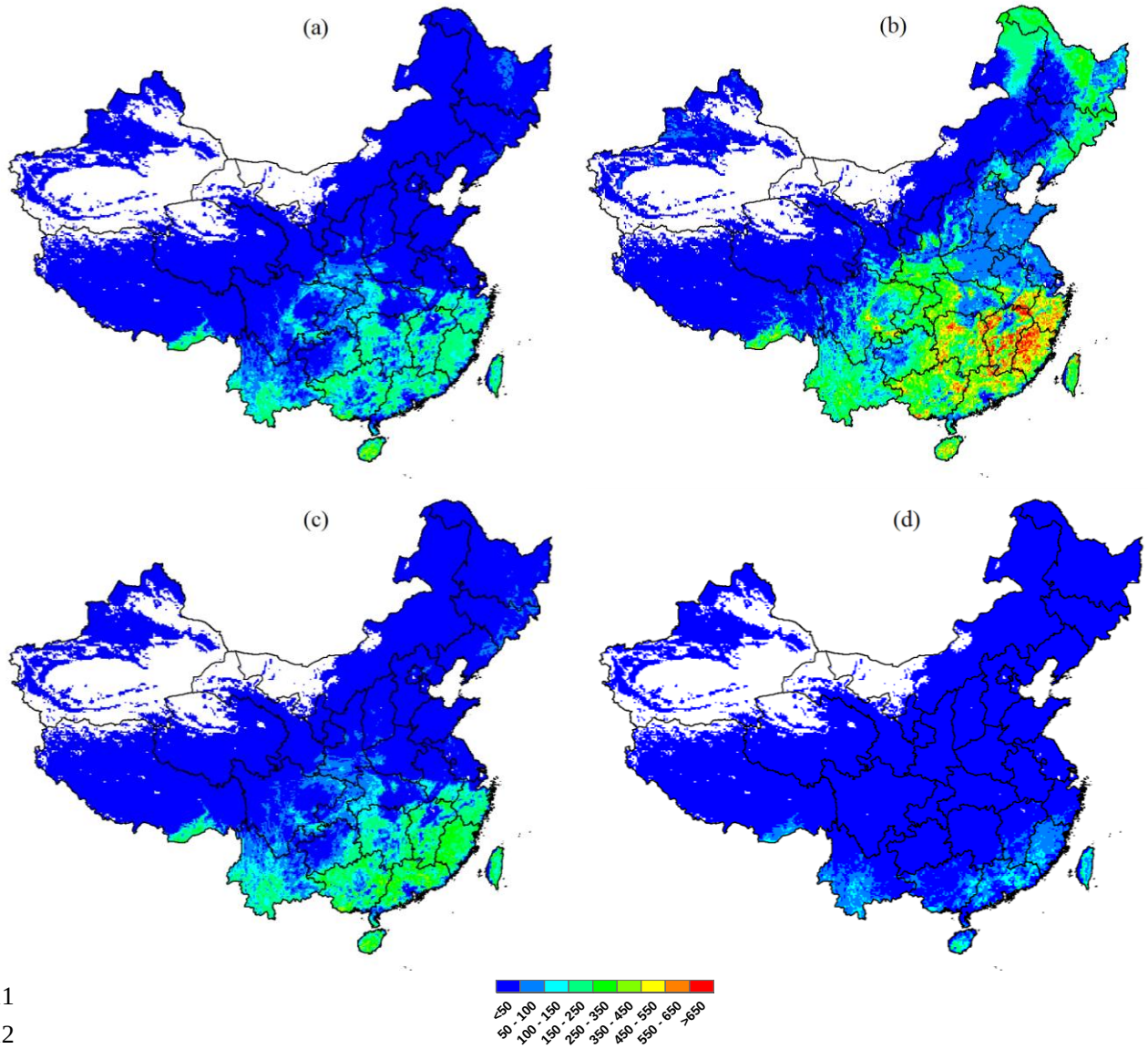

811

812

813 Fig. 7 Average (calculated) seasonal monoterpenes emission fluxes (g C km^{-2} h^{-1}): (a)

814 spring; (b) summer; (c) autumn; (d) winter

815

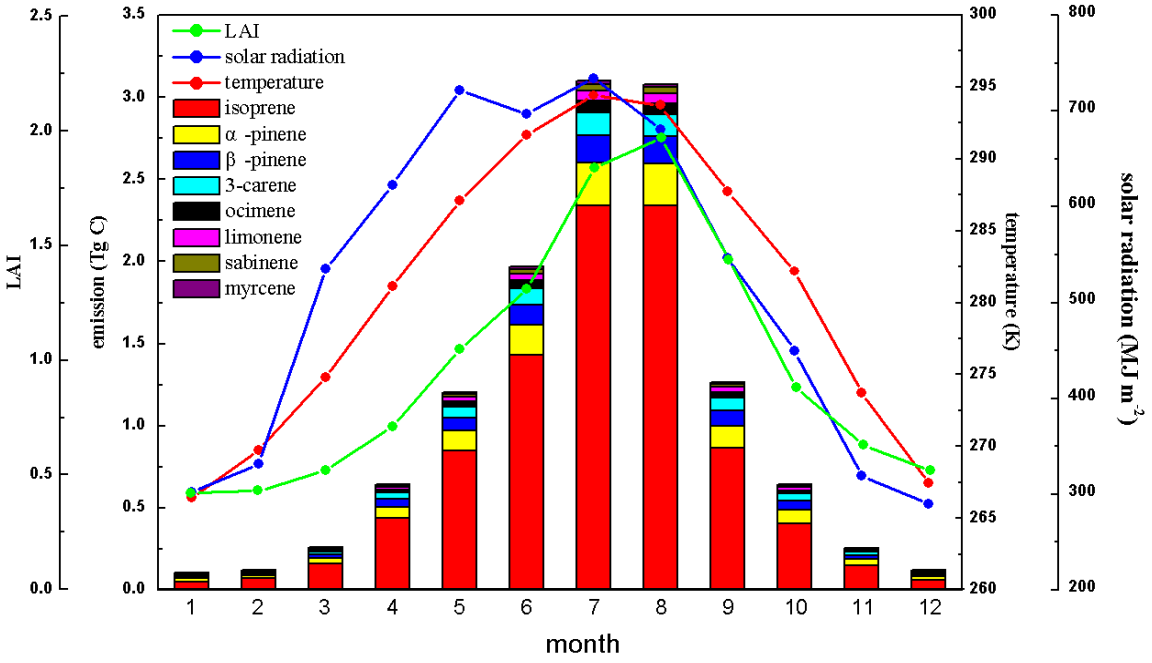

816

817 Fig. 8 Calculated monthly variation of BVOC emission rates of, LAI values,

818 temperatures at 2 m and solar radiation energy

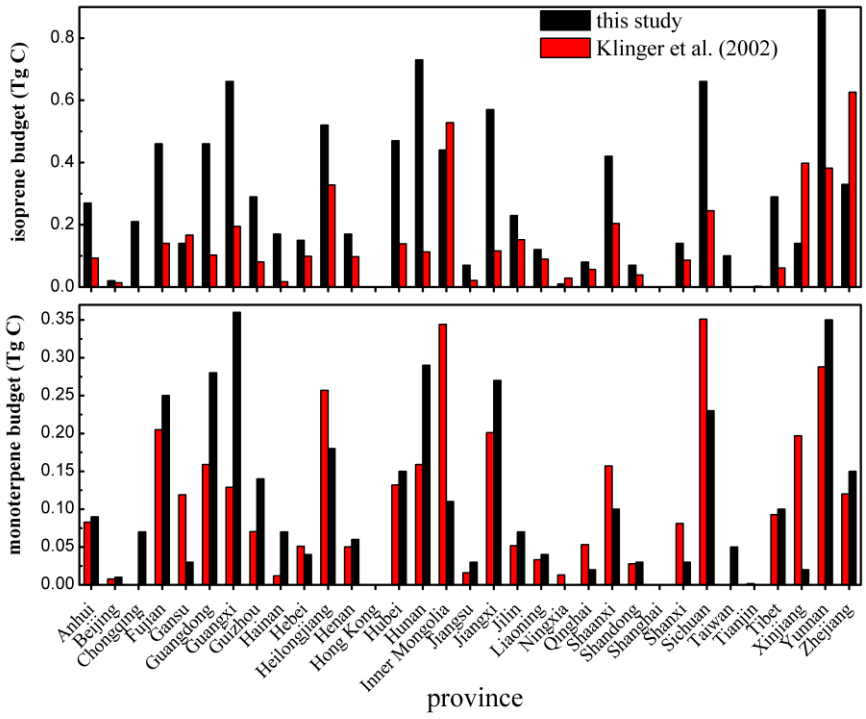

819

820 Fig. 9 Comparisons of province-level BVOC emissions in this study with Klinger et al.

821 (2002)